Fusion Engineering and Design 215 (2025) 114981

Contents lists available at ScienceDirect

Fusion Engineering and Design

journal homepage: www.elsevier.com/locate/fusengdes

Preliminary thermo-structural analyses of the new DTT bolometric camera

V. D'Agostino [a,d,*], A. Belpane [b,c], S. Palomba [e], E. Peluso [a,d], I. Wyss [a], B. Spolaore [b], I. Regoli [b,g], L. Gabellieri [e], A. Murari [b,e,f], G. Apruzzese [d], M. Gelfusa [a]

[a] Industrial Engineering Department, University of Rome Tor Vergata, Via del Politecnico 1, 00010 Rome, Italy
[b] Consorzio RFX (CNR, ENEA, INFN, Università di Padova, Acciaierie Venete SpA), Corso Stati Uniti 4, 35127 Padova, Italy
[c] Department of Economics, Engineering, Society and Business Organization, University of Tuscia, Largo dell'Università, 01100 Viterbo, Italy
[d] ENEA, Nuclear Department, Via Enrico Fermi 45, 00044 Frascati, Italy
[e] DTT S.c. a r.l., Via Enrico Fermi 45, 00044, Frascati, Italy
[f] Istituto per la Scienza e la Tecnologia dei Plasmi, CNR, Corso Stati Uniti 4, 35127, Padova, Italy
[g] Department of Civil and Industrial Engineering, University of Pisa, Via Girolamo Caruso, 8, Pisa, 56122, Italy

ARTICLE INFO

Keywords:
Bolometry
DTT
Diagnostics
FEM

ABSTRACT

The Divertor Tokamak Test (DTT) facility is currently under construction at the ENEA Frascati Research Centre, Italy, with the aim of studying divertor configurations in support to the design and construction of ITER and DEMO. In the context of monitoring the radiated power, it is crucial to measure the entire spectrum of electromagnetic radiation emitted by the plasma. This need is particularly relevant in the divertor region, especially in the specific case of DTT scientific programme. This work presents the preliminary thermal and structural analyses of the bolometric camera foreseen to be implemented in the tomographic diagnostic system, aimed at monitoring the emissivity of the plasma total radiated power. First, the design has been optimised, minimising the space occupied in the port by the arrays of metal foil bolometers, still ensuring the best possible coverage of the lines of sight (LoS) in the vessel and at the same time avoiding interferences with other devices. Then, the devised layout has been validated with thermo-mechanical simulations, focusing on the design of the active cooling system of the bolometers themselves, necessary to manage the thermal conditions of the wall, particularly baking, and the intense loads during machine operations. The results confirmed that, under the specific conditions of mirror polishing of components, the currently proposed layout is promising, but needs further optimisation.

1. Introduction

As part of the European EUROfusion roadmap [1], a key challenge is the development of efficient power dissipation solutions for the DEMO fusion power plant [2]. To address this challenge, the Italian DTT (Divertor Tokamak Test) project [3], currently underway at the ENEA research center in Frascati (Rome), is focused on exploring alternative divertor configurations, that can help optimize DEMO's design. To achieve its full potential, DTT will need a complete suite of diagnostic systems, including the bolometry, to measure plasma radiation and its spatial distribution. Bolometry provides a measure of the radiation emitted over a wide range of wavelengths, from X-rays to visible [4,5]. These detectors can provide line-integrated information directly or can be used for tomographic reconstructions, which allow the spatial distribution of the emissivity to be mapped [6]. Therefore, such measurements are used to retrieve the plasma energy balance and to support impurity transport [7].

This paper describes the mechanical layout of the bolometric camera for DTT and its preliminary thermomechanical simulations. The camera is currently under design and is based on commercial metal resistance bolometers, selected for their reliability and robustness [8]. Particular attention is devoted to an active bolometric cooling system, being necessary to manage the expected boundary conditions during DTT operations. For now, the choice of materials is oriented toward Au absorbers, SiN insulators and Pt meanders, with a guaranteed maximum operating temperature of at least 180 °C for the bolometric assembly.

Recognizing its key role, the bolometric diagnostic is widely used in many fusion devices, including MAST-U [5], JET [9,10], W-7X [11]. These machines use metal resistance bolometers, typically consisting of gold absorbers mounted on thin sheets of Mica, Kapton or SiN, with gold

* Corresponding author.
E-mail address: v.d.agostino@ing.uniroma2.it (V. D'Agostino).

https://doi.org/10.1016/j.fusengdes.2025.114981
Received 3 December 2024; Received in revised form 4 March 2025; Accepted 18 March 2025
Available online 28 March 2025

meanders on the opposite side [12]. The sensors foreseen to be employed in ITER are described in [13].

In a tokamak, bolometers are used for their reliability in measuring accurately the radiation emitted by the plasma. These instruments detect radiation through the temperature rise caused by the energy affecting a resistor in a Wheatstone bridge, transforming the variation in electrical resistance into a signal proportional to the absorbed radiation. Fig. 1 shows how a bolometer unit is assembled [14].

The integrated measurements are transformed into two-dimensional images of the plasma radiation distribution via tomographic reconstruction, which is essential for analysing how radiation is distributed and dissipated within the tokamak Vacuum Vessel (VV). In particular, understanding the emissivity distribution is crucial for operating the machine safely and for preventing disruptions [15,16].

The paper is organized as follows. Section 2 provides a comprehensive overview of the bolometric diagnostic camera, detailing both the mechanical design aspects and the fundamental heat exchange considerations, essential for its operation. Specifically, three case studies are reported, whose results are discussed in Section 3, while conclusions and plans for improving the diagnostic in the future are outlined in the final Section 4.

2. Mechanical layout

In addition to metal foil resistors, a bolometric unit comprises several critical components: a protective casing that insulates the device, ensuring precise measurements under extreme conditions; a slit aperture that defines the field of view, selectively collimating radiation to reduce interferences, from internal reflections, and provides the required spatial resolution, which is vital for capturing detailed radiation patterns emitted by the plasma. Lastly, an ECRH stray protection shield is employed to guard the bolometer against interference from stray microwaves generated by the ECRH system. In subSection 2A, the mechanical port of interest is presented, followed by the optimized mechanical bolometry configuration. In subSection 2B, the physics of the system is explored, including thermal analysis pre-processing and boundary conditions.

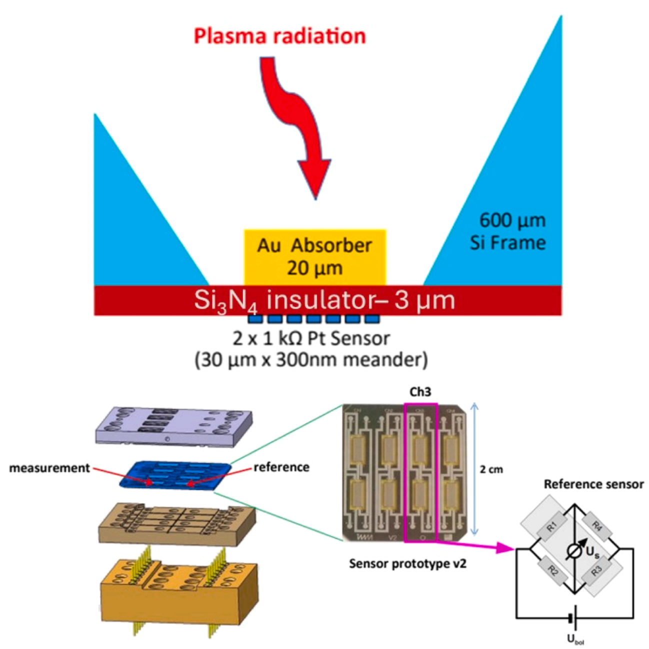

Fig. 1. in this figure [14], an example of schematization of a bolometric unit is reported, including the materials used, the assembly and its dimensions. The plasma radiation impinges on a 4–20 µm gold absorber, while a 3 µm insulator is employed to transfer the heat to the measuring resistors, integrated into a Wheatstone bridge configuration.

2.1. Optimized configuration in the equatorial port

The vacuum vessel (VV) of a tokamak provides several openings for the plasma diagnostic systems, the vacuum system etc. Specifically, in DTT VV, each standard module is equipped with five access ports. The bolometry is distributed on four ports (P1 to P4, while P5 is not relevant to this paper, since it is completely dedicated to support structure) [17], to perform both offline and real time tomographic reconstructions, whose numerical algorithms are under development and are detailed in [7]. Fig. 2 shows the diagnostic access points of each port with the coverage of the planned LoS.

The bolometric diagnostic is installed inside a chassis, a modular interface that ensures precise alignment of the instruments with respect to the plasma, providing a stable support while simultaneously allowing easy removal for maintenance. The diagnostic chassis is placed into the Port Plug, a robust and shielded structure, that, facing the plasma, provides protection against radiation and conducted heat [18].

This work focuses on P3, as it is the most critical. The criticality arises from the fact that this port is equatorial and therefore the diagnostics contained there are closer to plasma, hence more subject to radiation. Moreover, the space constraints are particularly severe due to the presence of other diagnostics, so a vertical arrangement of the bolometric camera is planned along the inner wall of the port. The available space in equatorial ports is then optimized, integrating the bolometric camera with the Soft-X diagnostic. In particular, both diagnostics are to be mounted on the two opposite sides of a single plate [18,19], as shown in Fig. 3.

The bolometric camera design, whose isometric view is illustrated in Fig. 4, consists of three main parts:

- Cooling system, including two $CuCr_1Zr$ [20] pipes, each of them made of a cylindrical and a rectangular body, to maximize the contact area with the bolometers.
- Port anchor structure (PAS) in AISI 316 L [21], which screws the system to the plate and has a footprint of 35.5 mm, not interfering with other diagnostics in the port (see Fig. 5).
- Array of commercial bolometric sensors.

The change in the water pipe section can be observed near the

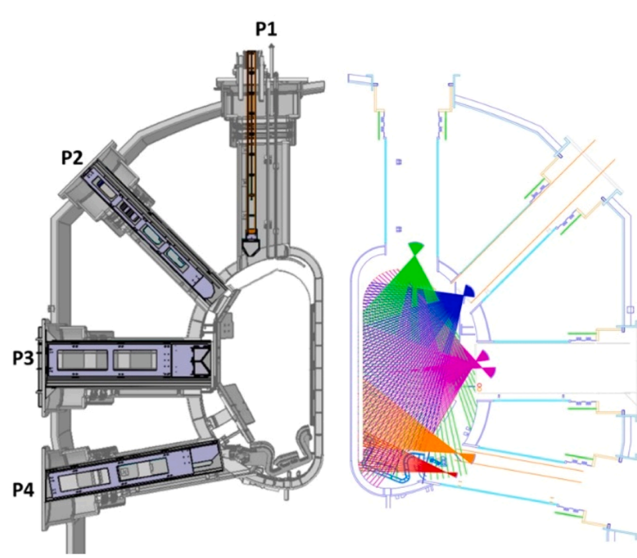

Fig. 2. The access ports P1 to P4 are shown. On the left, the mechanical layout of the ports is illustrated [18]. On the right, the lines of sight (LoS) under definition, as reported in [7], are depicted.

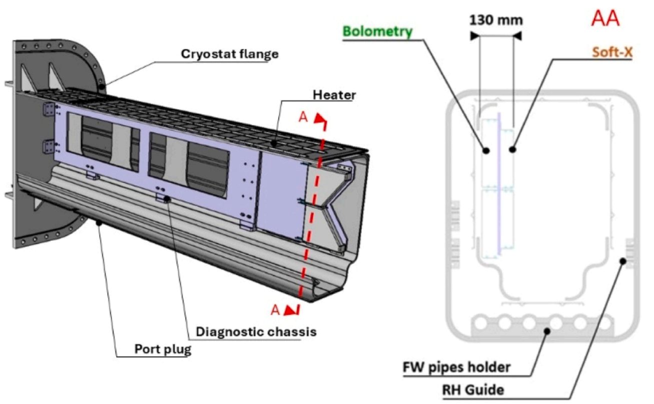

Fig. 3. An isometric view of Equatorial Port 3 is presented, along with the section view 'AA' of the port. The latter highlights the placement of the bolometric diagnostic box (see Section 4), mounted on a single plate alongside the soft-X diagnostic, in proximity of the first wall [18] (see Fig. 2).

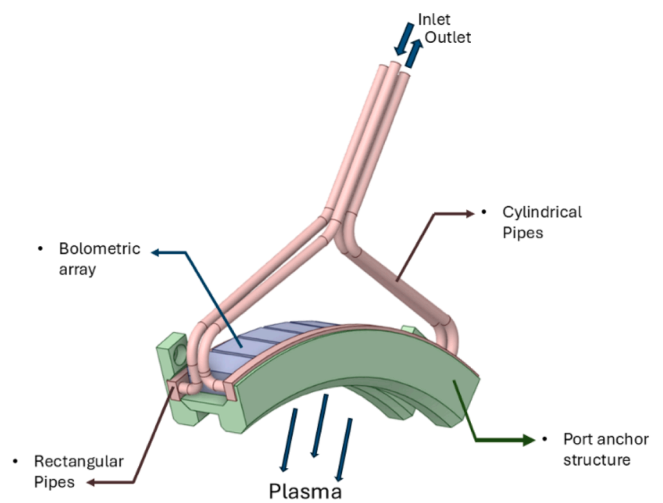

Fig. 4. Overview of the bolometric system, highlighting the cooling system in pink.

external bolometer. Inlet and outlet of water is also shown for a single pipe and the heat exchange is counterflow between the two sides. The PAS, depicted in green, consists of two sides that are mutually screwed together. In grey, the bolometric arrangement is illustrated, where the orientation of the grey face determines the geometric factor of the optical system. In Fig. 5A-B, the section views of the bolometric camera are

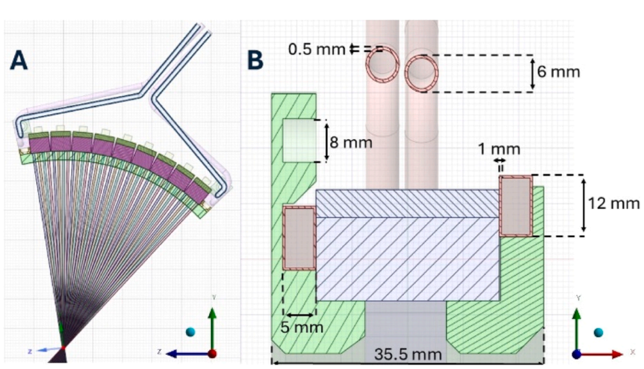

Fig. 5. Figure A shows the ZY section view with the distribution of LoS with respect to the plasma, figure B details the characterizing dimensions of the pipes in the cooling system and their footprint, in XY plane.

reported, including the distribution of LoS, the dimensions of the pipes and their footprint.

Fig. 5 also highlights the direct contact between the rectangular pipes and the bolometric unit, to ensure the best cooling. Also, the PAS anchors both pipes to the bolometric array and leaves the two resistances lines facing the plasma, without interfering with the optics of the system.

2.2. Simulation set-up

This paragraph discusses the physics of the system and focuses on boundary conditions of the analyses, whose results are discussed in Sec. 3. The thermal simulations include the forced convection on the internal pipes surface, with water as coolant. This has an internal average velocity of 2 m/s and an inlet temperature of 60 °C, plant design parameters of DTT. The convective Heat Transfer Coefficient (**HTC**) is determined using the Nusselt Number (**Nu**) via Gnielinski correlation. Nu represents the efficiency of convective versus conductive heat transfer in a system and is calculated analytically [22], considering the geometric characteristics of pipes and the inlet values of the cooling water. From the calculated Nu, which results about 149.20, the hydraulic diameter (d_i) of 5 mm, and the thermal conductivity (λ), the resulting HTC is of 9670 W/m²K and is estimated from the following formulas [22]:

$$HTC = \frac{Nu \cdot d_i}{\lambda} \tag{1}$$

$$C = 1.07 + \frac{900}{Re} - \frac{0.63}{1 + 10 \cdot Pr} \tag{2}$$

$$f = 0.079 \cdot Re^{0.25} \tag{3}$$

$$Nu = \frac{\frac{f}{2} \cdot Re \cdot Pr}{C + 12.7 \cdot \sqrt{\frac{f}{2}} \cdot \left(Pr^{0.6667} - 1\right)} \tag{4}$$

where C is a constant that considers the flow characteristics of the fluid through Reynolds Number Re, equal to ~20,000, defining turbulent regime, and the thermal properties of the fluid through the Prandtl Number Pr, whose value is 6.64 in this study. It is a correction factor that combines these two dimensionless numbers to reflect how heat transfers into the system under turbulent flow conditions; in this case, C results equal to around 1.10. In its turn, f is the Blasius friction coefficient and represents the resistance of the fluid flow due to the pipe's surface roughness and geometry; in these simulations is has the value of $6.65 \cdot 10^{-3}$. Regarding the structural simulations, the mechanical load is given by the 8-bar water circulating into the pipes, applied in the simulation as a normal pressure on their inner surfaces. The contacts have been tooled to consider screwing at the bolometer-structure front interface. In particular, the front faces of the bolometers are bolted on the structure to allow packet closure of the water pipes, which are instead inserted by side sliding between PAS and bolometers. For this reason, a friction coefficient of 0.5 has been considered between the side faces of bolometers, the rectangular pipes, and the PAS, to simulate eventual mutual rotations, which have also to be considered when sliding mounting the diagnostic. The empty holes are those indicated in Fig. 6, through which the sensor mount is attached to the camera support structure (in this case the PAS), ensuring package closure.

Finally, the structure is anchored to the inner wall of the port via the two openings in the PAS, simulated as fixed supports. Fixed supports are also installed at the extremities of the pipes to secure them to the structure. Fixed surfaces are shown in blue in Fig. 7. This constraint remains unchanged in all structural simulations, as maintenance of diagnostics does not involve disassembly of pipes.

Specific boundary conditions are discussed in the subSections 3.A, 3.B and 3.C.

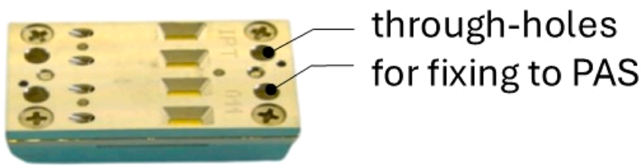

Fig. 6. The picture reports a single unit of the bolometric array shown in Fig. 4, with front plate (top), back plate, and ground plate. The latter typically contains the spring-loaded pins to ensure the electrical contact of the sensors and is attached to the front plate-sensor-back plate stack by the four bolts, whose heads are visible in the corners of the front plate.

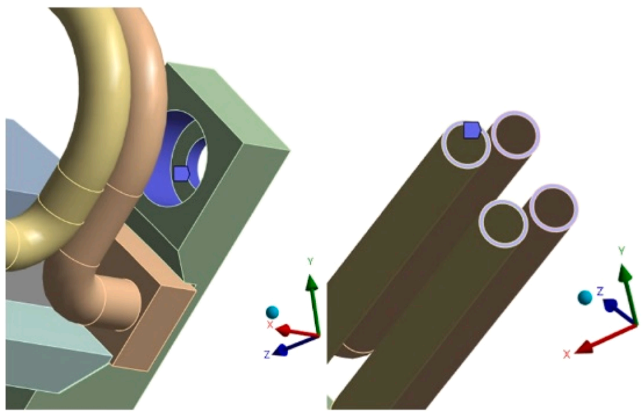

Fig. 7. The figure shows the boundary condition of fixed support, applied on the holes on the PAS which are dedicated to screws and on the extremities of pipes.

3. Thermo-structural verifications and results

In this section, the results of the thermo-structural analysis, performed with the software Ansys®, via the Workbench interface [23], are presented. In thermal simulations, the monitored parameter is temperature. In contrast, the structural simulations evaluate the deformations, expressed as the maximum displacement from the original configuration and computed as the Euclidean norm of the three directional displacement components. Additionally, the structural simulations provide equivalent stresses according to the Von Mises criterion [24].

3.1. Baking

The first analysis presented regards the baking, that is an effective wall conditioning method. It allows removing the water, volatile hydrocarbons, and hydrogen through thermal desorption by increasing the temperature of the vacuum vessel. In DTT a high-temperature fluid, hot nitrogen, will be circulated inside the doubled wall of the VV to perform the baking [25]. In this analysis, the baking temperature is set at 250 °C for conservative reasons (the maximum design baking temperature is 200 °C in DTT) and operates uniformly on the entire camera, while the bolometer cooling is always active. The boundary conditions are then radiation to ambient at 250 °C, set to each external surface, as shown in blue in Fig. 8, and water convection within the pipes. In particular, baking affects all the external surfaces in the bolometric camera.

This simulation is to be intended at steady state, since the interval at final temperature is foreseen to last around 24 h in the short-term maintenance (STM) [25]. Results at the end of the baking time are reported in Tables 1 and 2.

Fig. 9 depicts how temperature distribution appears on bolometric array, in consequence of the action of both radiation and convection given by the cooling system. In particular, the lowest temperatures are located near the cooling pipes and present a gradient, in both the toroidal and plasma facing directions. The cooling system is not influenced by the baking and keeps the water inlet temperature of 60 °C.

For what regards mechanical behaviour of the model under baking conditions, maximum stresses are concentrated at the pipe change of section, where there is the variation from cylindrical to rectangular

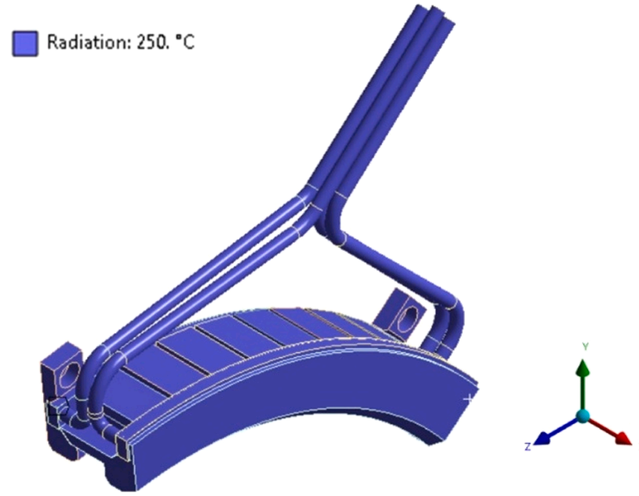

Fig. 8. The figure shows in blue all the surfaces where the boundary condition of radiation (to ambient), to simulate baking process, is applied.

Table 1
The table reports the reached temperature in case of baking at 250 °C.

Baking at 250 °C	Bolometers T_{max}	PAS T_{max}	Pipes T_{max}
Thermal results	~61 °C	~65 °C	~60 °C

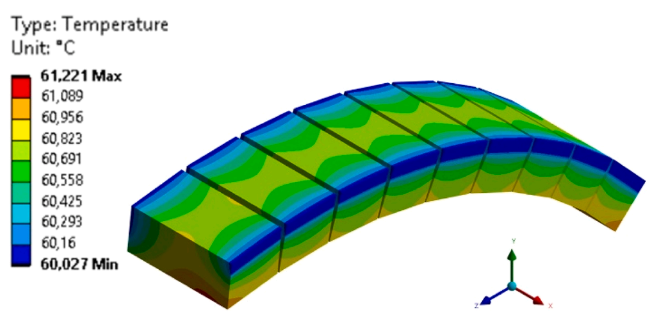

Fig. 9. The figure exhibits the distribution of temperatures on the bolometric array in case of baking.

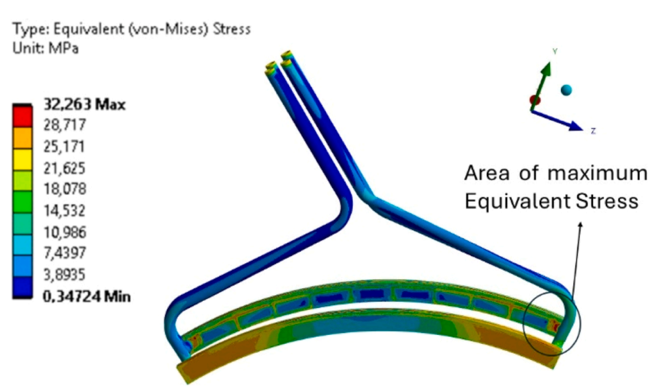

Fig. 10. This figure outlines the distribution of stress (MPa) on the cooling system pipes, in case of baking.

Table 2
The table illustrates the stresses and deformations experienced by the components during baking operation.

Baking at 250 °C	σ_{max} pipes	σ_{max} bolometers	σ_{max} PAS	Total Deformation
Mechanical Results	~32 MPa	~6 MPa	~29 MPa	~0.012 mm

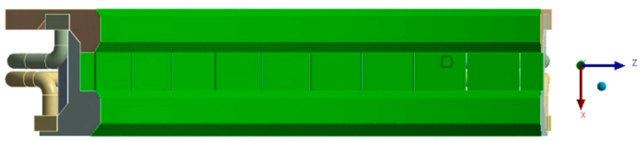

Fig. 11. The figure displays the faces of the PAS and bolometric array on which plasma thermal flux is applied, valid for both plasma scenario simulations (3.B, 3.C).

section, as depicted in Fig. 10.

From the results obtained, as reported in Tables 1 and 2, the proposed design presents no difficulties in handling loads during baking operation and the bolometric array is not affected by significant stresses.

3.2. Plasma pulse conditions with emissivity $\varepsilon = 0.2$ (0.1 MW/m^2)

The second analysis simulates the behaviour of the camera model during the 3600-seconds DTT cycle time at plasma target performance [3]. The DTT plasma discharge [26] lasts 100 s and includes start-up, ramp-up, flat-top and ramp-down phases. For a conservative approach, the entire 100-second duration is treated as if the plasma were in the flat-top phase only, to prioritize safety in the analysis. The cooling system remains operational throughout the entire 3600-seconds cycle.

The nominal heat load of DTT plasma is 0.5 MW/ m^2 due to the plasma radiation emission [3]. In this realistic case, it is assumed that part of the heat flux is reflected by the surface, which has been subjected to grinding, resulting polished. Specifically, the emissivity (ε) of components has a value of 0.2 [27], meaning that only 20 % of the total heat flux of 0.5 MW/m^2 is absorbed, resulting in an absorbed flux of 0.1 MW/m^2. In Fig. 11, the green faces stand for the ones looking directly to the plasma, on which the heat flux is applied in the thermal simulation as boundary condition. The same condition persists in the simulation described in subSection 3.C.

Table 3
The table shows the resulting temperatures for a surface grid configuration, assuming an emissivity of $\varepsilon = 0.2$.

$\varepsilon = 0.2$ (0.1 MW/m^2)	Bolometer T_{max}	PAS T_{max}	Pipes T_{max}
Thermal results	~169 °C	~226 °C	~60 °C

This simulation has been conducted using a solver-controlled time step, with a maximum of 10 s in the plasma phase (0–100 s) and of 350 s in the cooling phase (100–3600 s), to adequately capture the transient thermal behaviour of the system, as for the scenario depicted in 3.C.

The corresponding temperatures are presented in the Table 3.

The temperature distribution on the bolometric array is reported in Fig. 12.

The upper figure highlights the distribution of temperature on the plasma-exposed faces, while the lower figure shows the distribution on the isometric view. Notably, the temperature decreases proportionally as the distance from the plasma increases, with temperatures around 60 °C in proximity of the cooling system pipes, due to the action of water. Also noticeable is a temperature gradient of around 8 °C between the line of measuring resistors and the line of cooling resistors, in toroidal direction, due to the different height of the pipes, which unbalances the cooling on one side. In case of plasma pulse, the maximum temperature is time-dependent and is reached after 100 s of plasma heat flux, as shown in Fig. 13. From the following instant onward, the temperature begins to decrease, as there is no longer any thermal load from the plasma, only the action of the water-cooling system. In Fig. 13, it is possible to see that the temperature stabilizes again at 60 °C at about 700 s.

With such temperatures, resultant stresses and deformation are those reported in the following Table 4.

Most of the deformation is concentrated near the cooling system due to the internal pressure of the pipes, in the rectangular area, as expected, due to the presence of sharp edges. Distributions of deformation values are reported in Fig. 14.

It therefore confirms that, in this realistic scenario, the system can handle the thermo-structural load, considering the operating range of the materials in use [20,21] and the maximum operative temperature of commercial bolometers assembly, that is 180 °C.

3.3. Plasma pulse conditions with emissivity $\varepsilon = 1$ (0.5 MW/m^2)

In this case, the black-body assumption has been adopted, as the emissivity (ε) of materials generally decreases with increasing temperature. In reality, emissivity is typically <1 and depends on several factors, including temperature, wavelength, and surface characteristics. Most materials exhibit reduced emissivity at higher temperatures, which influences their thermal radiation when compared to an ideal black

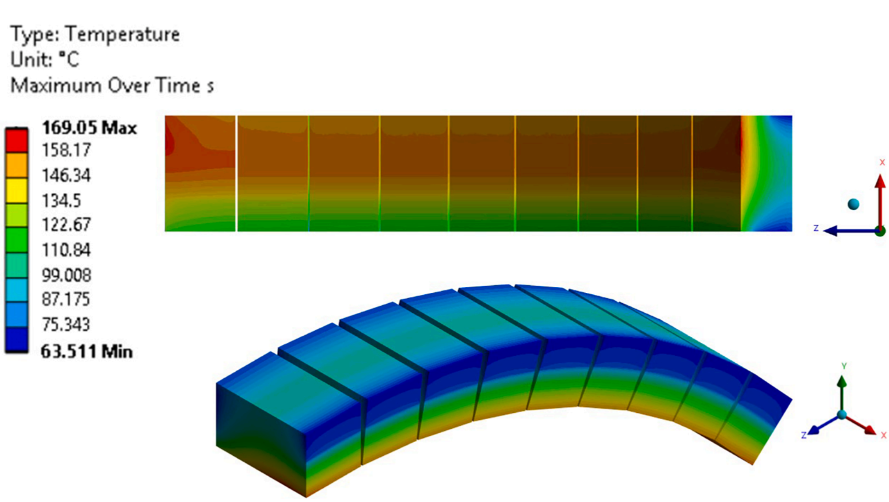

Fig. 12. The distribution of temperature on the bolometric array at $\varepsilon = 0.2$ is profiled.

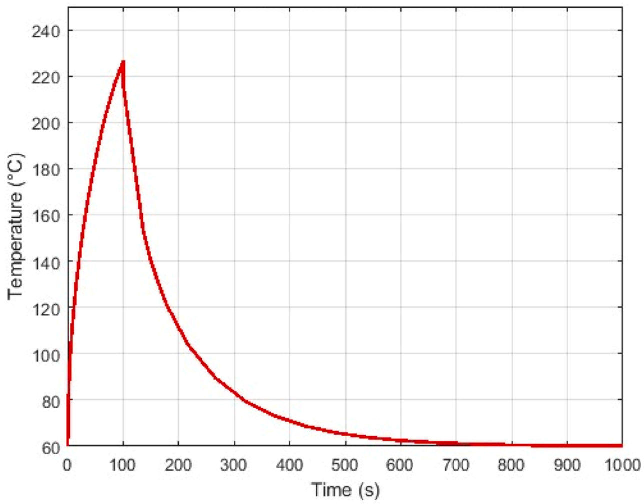

Fig. 13. The plot represents the temperature increase on PAS.

Table 4
The table presents the mechanical results for components with an emissivity of $\varepsilon = 0.2$ and an incident heat flux of 0.1 MW/m^2.

$\varepsilon = 0.2$ (0.1 MW/m^2)	σ_{max} pipes	σ_{max} bolometers	σ_{max} PAS	Total Deformation
Mechanical results	~46 MPa	~35 MPa	~38 MPa	~0.026 mm

body [28]. In the model, an emissivity of 1 is assumed, allowing it to fully absorb the nominal 0.5 MW/m^2 DTT plasma heat flux [3]. This represents the most conservative scenario, with the corresponding results presented in Table 5:

As the boundary conditions are equivalent to scenario 3.B, except for the numerical value, this simulation gives the same temperature distribution and time-dependency analysed in the previous subsection. Except on pipes, temperatures reached on both PAS and bolometric array are critical. This poses risks not only to the integrity of the PAS, as AISI 316 L can operate effectively up to 800–850 °C, making this a severe limit condition, but also to the operating conditions of the bolometers, which could not survive 600 °C. Given the temperatures achieved, which are above the thermal integrity limits of the constituent materials, further structural analysis would not be useful as the system cannot operate under these conditions.

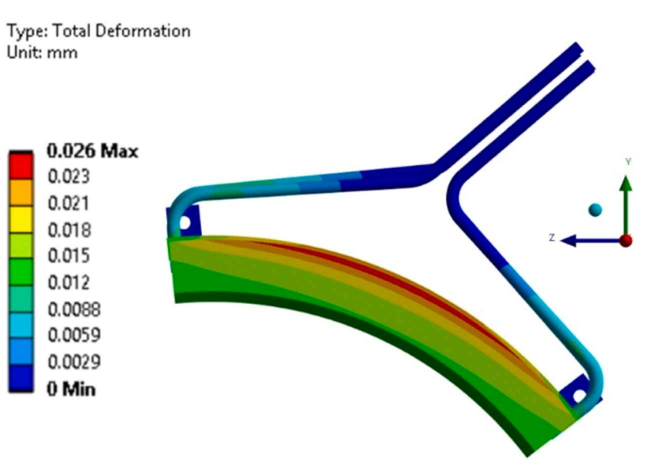

Fig. 14. The distribution of deformation for the model with $\varepsilon = 0.2$ is depicted. In particular, the maximum occurred in the model is represented in red in the distribution.

Table 5
This table presents the temperatures of the components assuming total absorption of the heat flux, consistent with black body behaviour.

$\varepsilon = 1$ (0.5 MW/m^2)	Bolometer T_{max}	PAS T_{max}	Pipes T_{max}
Thermal results	~620 °C	~830 °C	~60 °C

4. Conclusions and future developments

The analysis of DTT bolometric diagnostic has shown promising results and has provided useful indications for optimizing the design and operation of the system. Despite the high operating temperatures in a tokamak, the cooling system designed for the bolometers has proved to keep temperatures within acceptable limits in specific conditions. In realistic simulations indeed, with 0.1 MW/m^2 plasma flux hitting the structure, the peak simulated temperature on the bolometers is about 169 °C. Also, during baking conditions the maximum temperature is registered on the PAS, which reaches 65 °C, largely tolerable; Also, in both structural scenarios, safety is guaranteed for the maximum stresses and deformations, for their values are far from tensile yield. These values indicate that the camera assembly can handle the thermal load during standard operations. The materials selected, $CuCr_1Zr$ for the cooling pipes and 316 L stainless steel for the PAS, have proved suitable for this application. $CuCr_1Zr$ provides good thermal conductivity, while 316 L stainless steel supplies structural strength and thermal resistance.

Although the observed temperatures are within operational limits under realistic assumptions, an extremely conservative approach is adopted using the blackbody hypothesis. Requiring the assembly to withstand even the loading conditions associated with this hypothesis, this implies that a further optimization is needed. Improvements in materials or cooling system efficiency could help to further reduce the temperature spikes, increasing the longevity of the camera and improving the measurement accuracy. The first optimization to be explored is the placement of the pipes at the same height; to symmetrize cooling and avoid temperature gradients between measurement and reference resistor. Indeed, to ensure the proper operation of the bolometers, the same conditions, except for the plasma irradiation, have to be applied to both the reference and measuring sensors.

Moreover, the addition of an active cooled metallic box, integrating the optical pinhole and mesh shield for ERCH stray radiation; such box will be used as protection of the slit, to minimize deformation on the latter and to reduce the PAS height. The box model is currently under development and testing.

The presence of the box is therefore an additional protection to mitigate the effect of the plasma heat flux and provide more reliable thermal control. This intervention can then increase the heat distribution and reduce the maximum temperatures reached by the bolometers, thereby increasing the safety and reliability of the camera.

The results of the study are encouraging and indicate that the bolometry housing system is robust, well positioned to meet the needs of the DTT. With the appropriate optimizations, including adjustments of the bolometer arrays to match other ports, the system can contribute crucially to diagnosing the plasma, improving the understanding of physical phenomena and supporting the overall success of the DTT project.

CRediT authorship contribution statement

V. D'Agostino: Writing – original draft, Validation, Methodology, Investigation, Formal analysis, Data curation, Conceptualization. **A. Belpane:** Writing – review & editing, Visualization, Validation, Supervision, Methodology, Data curation, Conceptualization. **S. Palomba:** Writing – review & editing, Visualization, Conceptualization. **E. Peluso:** Writing – review & editing, Software. **I. Wyss:** Writing – review & editing, Resources. **B. Spolaore:** Software. **I. Regoli:** Writing – review &

editing, Software. **L. Gabellieri:** Writing – review & editing, Project administration. **A. Murari:** Writing – review & editing, Supervision. **G. Apruzzese:** Writing – review & editing, Project administration. **M. Gelfusa:** Writing – review & editing, Supervision.

Declaration of competing interest

The authors declare that they have no known competing financial interests or personal relationships that could have appeared to influence the work reported in this paper.

Data availability

Data will be made available on request.

References

[1] M. Turnyanskiy, et al., European roadmap to the realization of fusion energy: mission for solution on heat-exhaust systems, Fusion Eng. Design (2015) 96–97, https://doi.org/10.1016/j.fusengdes.2015.04.041. Volumes.
[2] E. Joffrin, et al., Overview of the EUROfusion Tokamak Exploitation programme in support of ITER and DEMO, Nucl. Fusion 64 (2024) 112019, https://doi.org/10.1088/1741-4326/ad2be4.
[3] F. Romanelli, et al., Divertor Tokamak Test facility project: status of design and implementation, Nucl. Fusion 64 (2024) 112015, https://doi.org/10.1088/1741-4326/ad5740.
[4] E.R. Müller, F. Mast, et al., A new metal resistor bolometer for measuring vacuum ultraviolet and soft x radiation, J. Appl. Phys. 55 (1984) 2635–2641, https://doi.org/10.1063/1.333272.
[5] J. Lovell, et al., Overview and first measurements of the MAST Upgrade bolometer diagnostic, Rev. Sci. Instrum. 94 (2023) 023509, https://doi.org/10.1063/5.0128750.
[6] M. Odstrcil, et al., Modern numerical methods for plasma tomography optimisation, Nucl. Inst. Methods Phys. Res. A 686 (2012) 156–161, https://doi.org/10.1016/j.nima.2012.05.063.
[7] E. Peluso et al., "Maximum likelihood bolometric tomography for DTT diagnostic design", to be submitted to FED.
[8] G. Apruzzese et al., "The updated bolometric diagnostic design for DTT", Proceedings P5.043 EPS 2024.
[9] A. Huber, et al., Upgraded bolometer system on JET for improved radiation measurements, Fusion Eng. Design (2007), https://doi.org/10.1016/j.fusengdes.2007.03.027.
[10] A. Murari, E. Peluso, et al., Investigating the thermal stability of highly radiative discharges on JET with a new tomographic method, Nucl. Fusion 60 (2020) 046030, https://doi.org/10.1088/1741-4326/ab7536.
[11] D. Zhang, et al., Design criteria of the bolometer diagnostic for steady-state operation of the W7-X stellarator, 2010, Rev. Sci. Instrum. 81 (2010) 10E134, https://doi.org/10.1063/1.3483194.
[12] K.F. Mast, et al., A low noise highly integrated bolometer array for absolute measurement of VUV and soft x radiation, Rev. Sci. Instrum. 62 (1991) 744–750, https://doi.org/10.1063/1.1142078.
[13] S. Jahanbakhsh, et al., Calibration and thermal test results of prototype bolometer sensors for ITER fusion reactor, Rev. Sci. Instrum. 94 (2023) 033503, https://doi.org/10.1063/5.0134449.
[14] H. Meister, et al., Bolometer developments in diagnostics for magnetic confinement fusion, JINST 14 (2019) C10004, https://doi.org/10.1088/1748-0221/14/10/C10004.
[15] B. Sieglin, et al., Disruption avoidance and investigation of the H-mode density limit in ASDEX upgrade, Plasma Phys. Control Fusion 66 (2024) 025004, https://doi.org/10.1088/1361-6587/ad163a.
[16] I. Wyss et al., "Comparison of a fast low spatial resolution inversion method and peaking factors for the detection of anomalous radiation patterns and disruption prediction," 2023, DOI 10.1016/j.fusengdes.2023.113625.
[17] R. Martone et al., "Divertor Tokamak Test Facility INTERIM report", DTT Green Book (dtt-project.it).
[18] A. Belpane et al., "Mechanical design of the new bolometric and soft-X ray diagnostics for DTT", ICFDT7 Poster, to be submitted to JINST.
[19] S. Palomba et al., "Conceptual design of Soft X-ray tomography system for DTT", to be submitted to FED.
[20] Metalcor, "Datasheet CuCrZr", CuCr1Zr, C18150 | Datasheet | METALCOR.
[21] Atlats Steel, "Stainless steel 316, 316L, 316H grade data sheet", 2021, Stainless Steel 316, 316L, 316H Grade Data Sheet.
[22] Ramesh K. Shah and Dušan P. Sekulic, Fundamentals of heat exchange and design, Sixth Edition, https://onlinelibrary.wiley.com/doi/book/10.1002/9780470172605?msockid=0613a2594da46e3c2851b7674c796f6d.
[23] Ansys Workbench | Simulation Integration Platform.
[24] Y. Huang, et al., A generalized von Mises criterion for yield and fracture, J. Appl. Mech. (Jun 1980), https://doi.org/10.1115/1.3153658.
[25] G. Rubino et al., "Design analysis of the DTT wall conditioning systems," in IEEE Trans. Plasma Sci., DOI: 10.1109/TPS.2024.3442482.
[26] R. Albanese, "DTT: a divertor tokamak test facility for the study of the power exhaust issues in view of DEMO", DOI 10.1088/0029-5515/57/1/016010.
[27] Surface emissivity coefficients, Engineering Toolbox, https://www.engineeringtoolbox.com/emissivity-coefficients-d_447.html.
[28] Frédéric Valiorgue, et al., Emissivity calibration for temperatures measurement using thermography in the context of machining, Appl. Therm. Eng. 58 (2013), https://doi.org/10.1016/j.applthermaleng.2013.03.051.